

# Role of magnetic ions in the thermal Hall effect of the paramagnetic insulator $\text{TmVO}_4$

Ashvini Vallipuram<sup>\*,†</sup>, Lu Chen<sup>\*,‡</sup>, Emma Campillo,<sup>1</sup> Manel Mezidi,<sup>1,2</sup> Gaël Grissonnanche,<sup>3,4</sup> Marie-Eve Boulanger,<sup>1</sup> Étienne Lefrançois,<sup>1</sup> Mark P. Zic,<sup>5</sup> Yuntian Li,<sup>6</sup> Ian R. Fisher,<sup>6</sup> Jordan Baglo,<sup>1</sup> and Louis Taillefer<sup>1,7,§</sup>

<sup>1</sup>*Institut quantique, Département de physique & RQMP,  
Université de Sherbrooke, Sherbrooke, Québec J1K 2R1 Canada*

<sup>2</sup>*Université Paris-Cité, Laboratoire Matériaux et Phénomènes Quantiques, CNRS (UMR 7162), 75013 Paris, France*

<sup>3</sup>*Laboratory of Atomic and Solid State Physics, Cornell University, Ithaca, NY 14853, USA*

<sup>4</sup>*Kavli Institute at Cornell for Nanoscale Science, Ithaca, NY 14853, USA*

<sup>5</sup>*Geballe Laboratory for Advanced Materials and Department of Physics, Stanford University, CA 94305, USA*

<sup>6</sup>*Geballe Laboratory for Advanced Materials and Department of Applied Physics, Stanford University, CA 94305, USA*

<sup>7</sup>*Canadian Institute for Advanced Research, Toronto, Ontario M5G 1M1, Canada*

(Dated: June 17, 2024)

In a growing number of materials, phonons have been found to generate a thermal Hall effect, but the underlying mechanism remains unclear. Inspired by previous studies that revealed the importance of  $\text{Tb}^{3+}$  ions in generating the thermal Hall effect in a family of pyrochlores, we investigated the role of  $\text{Tm}^{3+}$  ions in  $\text{TmVO}_4$ , a paramagnetic insulator with a different crystal structure. We observe a negative thermal Hall conductivity in  $\text{TmVO}_4$  with a magnitude such that the Hall angle,  $|\kappa_{xy}/\kappa_{xx}|$ , is approximately  $1 \times 10^{-3}$  at  $H = 15$  T and  $T = 20$  K, typical for a phonon-generated thermal Hall effect. In contrast to the negligible  $\kappa_{xy}$  found in the nonmagnetic pyrochlore analog (where the  $\text{Tb}^{3+}$  ions are replaced with  $\text{Y}^{3+}$ ), we observe a negative  $\kappa_{xy}$  in  $\text{YVO}_4$  with a Hall angle of magnitude comparable to that of  $\text{TmVO}_4$ . This shows that the  $\text{Tm}^{3+}$  ions are not essential for the thermal Hall effect in this family of materials. Interestingly, at an intermediate Y concentration of  $x = 0.3$  in  $\text{Tm}_{1-x}\text{Y}_x\text{VO}_4$ ,  $\kappa_{xy}$  was found to have a positive sign, pointing to the importance of impurities in the thermal Hall effect of phonons.

## I. INTRODUCTION

In the last decade, a thermal Hall effect has been measured in a number of insulators where phonons are the main heat carriers, including multiferroics such as  $\text{Fe}_2\text{Mo}_3\text{O}_8$  [1], cuprates such as  $\text{La}_2\text{CuO}_4$  [2, 3] and  $\text{Nd}_2\text{CuO}_4$  [4], nonmagnetic  $\text{SrTiO}_3$  [5] and the antiferromagnet  $\text{Cu}_3\text{TeO}_6$  [6], see Fig. 1. In  $\text{Tb}_3\text{Ga}_5\text{O}_{12}$  [7], the first insulator in which a thermal Hall signal was detected, the effect was attributed to skew scattering of phonons by superstoichiometric  $\text{Tb}^{+3}$  impurities [8].

Since then, a number of theoretical scenarios have been proposed to explain the origin of the phonon thermal Hall effect. Some attribute the thermal Hall conductivity  $\kappa_{xy}$  to the Berry curvature of phonon bands [9]. Others link it to various types of spin-lattice coupling [10–13]. In yet others, the role of impurities is considered important [14–16]. But it remains unclear which of these scenarios applies to what material.

In a previous study on pyrochlores [17], a sizeable  $\kappa_{xy}$  was observed in  $\text{Tb}_2\text{Ti}_2\text{O}_7$  but a negligible  $\kappa_{xy}$  was detected in  $\text{Y}_2\text{Ti}_2\text{O}_7$ . Although the  $\kappa_{xy}$  signal in  $\text{Tb}_2\text{Ti}_2\text{O}_7$  was originally attributed to some exotic neutral excitations linked to the spin-liquid nature of the system [17], it was later argued that phonons are in fact responsible for the thermal Hall effect in this ma-

terial [18], since a  $\kappa_{xy}$  signal of comparable magnitude is still observed when 70% of the  $\text{Tb}^{3+}$  ions are replaced by  $\text{Y}^{3+}$  ions, and the spin state of the system is profoundly altered. Irrespective of the underlying mechanism, this study does show that  $\text{Tb}^{3+}$  ions are essential for generating a thermal Hall effect in these pyrochlores.

Here we report a similar study carried out on a different oxide,  $\text{TmVO}_4$ , wherein we investigate what happens to the thermal Hall effect when we substitute the magnetic ion  $\text{Tm}^{3+}$  for the nonmagnetic ion  $\text{Y}^{3+}$ .

The insulator  $\text{TmVO}_4$  exhibits a rich set of phenomena at low temperatures. It undergoes a cooperative Jahn-Teller phase transition at  $T = T_D \simeq 2$  K in zero field, and at  $H = H_D \simeq 0.5$  T at  $T = 0$  (for  $H//c$ ) [24]. (Note that we use  $H$  as a shorthand notation for  $\mu_0 H$ .) The ordered state consists of a simultaneous ferroquadrupole order of the local 4f electronic orbitals of each Tm atom, accompanied by a structural transition, by which the crystal structure goes from tetragonal at high temperatures (I41/amd spacegroup [21]) to orthorhombic at low temperatures [24–28]. However, no magnetically ordered state has been reported in  $\text{TmVO}_4$  [24]. Our own study will focus on temperatures above  $T_D$ .

## II. METHODS

### A. Samples

The following three rare-earth vanadates were studied:  $\text{TmVO}_4$ ,  $\text{YVO}_4$  and  $\text{Tm}_{0.7}\text{Y}_{0.3}\text{VO}_4$ . The samples were grown using a flux growth method [29, 30]. They are nee-

<sup>†</sup>\* A.V. and L.C. contributed equally to this work.; ashvini.vallipuram@usherbrooke.ca

<sup>‡</sup> lu.chen@usherbrooke.ca

<sup>§</sup> louis.taillefer@usherbrooke.ca

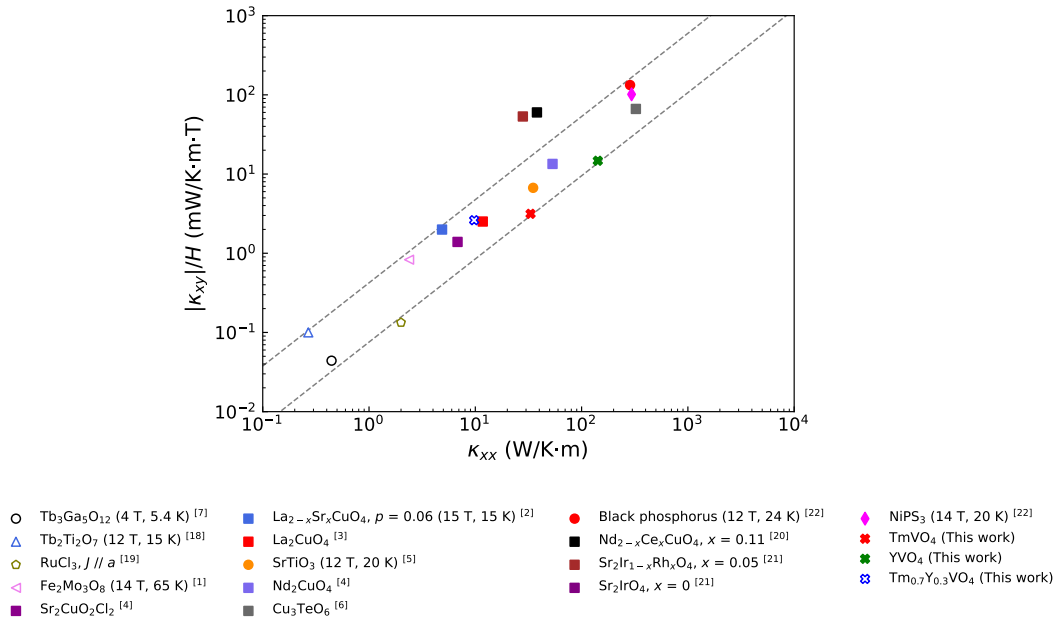


FIG. 1. Phonon thermal Hall conductivity normalized by field,  $|\kappa_{xy}|/H$  of various insulators [1, 3–7, 18–22] as a function of their thermal conductivity,  $\kappa_{xx}$ . The data are taken at  $H = 15$  T and  $T = 20$  K unless indicated otherwise. This figure is inspired from a similar plot from Li et al. [23] with the values of our three samples added. The grey lines mark the region where most values of  $\kappa_{xy}$  are found, showing that  $\kappa_{xy}$  scales with  $\kappa_{xx}$ , as emphasized previously [1, 2, 6, 23]. The two data points that lie above the delimited region are  $\text{Nd}_{2-x}\text{Ce}_x\text{CuO}_4 : x = 0.11$  [20] and  $\text{Sr}_2\text{Ir}_{1-x}\text{Rh}_x\text{O}_4 : x = 0.05$  [21] (see text). Open (full) symbols indicate a positive (negative)  $\kappa_{xy}$ .

dle shaped with their long axis along the  $c$  axis, which is the easy axis of magnetization [31]. Because  $\text{TmVO}_4$  has a large anisotropy in its  $g$ -factor ( $g_c = 10$  &  $g_a = g_b = 0$ ) [32], even a slight misalignment of the magnetic field can cause a large torque on the sample, which can detach from its mount.

Two measures were adopted to prevent this. First, the thermal transport contacts on  $\text{TmVO}_4$  and  $\text{Tm}_{0.7}\text{Y}_{0.3}\text{VO}_4$  samples were made with silver epoxy to ensure strong contacts that would adhere to a very smooth surface and wouldn't peel off. These contacts were solidified for about 10 minutes on a hot plate at 150 °C. Note that the contacts on the  $\text{YVO}_4$  samples were done with silver paint, since there is no magnetic torque in this case. For the heater contact, a 50  $\mu\text{m}$  diameter silver wire was used and for the thermal transport contacts, wires with a diameter of 25  $\mu\text{m}$  were used.

In addition, a small wood stick was positioned along the  $\text{TmVO}_4$  and  $\text{Tm}_{0.7}\text{Y}_{0.3}\text{VO}_4$  samples, and was linked to the sample by the heater wire. The thermal conductivity  $\kappa_{xx}$  was measured with and without the wood stick and only a 5 % (8 %) difference was observed at the peak temperature for  $\text{TmVO}_4$  ( $\text{Tm}_{0.7}\text{Y}_{0.3}\text{VO}_4$ ). The sample dimensions (contact dimensions) are given in Table I.

## B. Thermal transport measurements

To perform a conventional thermal transport study, a 5-contact measurement is done using a steady-state method at a fixed field, as sketched in Fig. 2. A heat current ( $\vec{J}$ ) is generated along the  $x$  axis from the heater contact on one end of the sample and the copper block on the other end. The heater is a strain gauge of 5 kΩ whose resistance does not change with temperature or field. (No potential strain is conferred to the sample since the heater is glued with GE varnish to a silver pad.) This heat current was applied along the  $c$  axis of the sample (the  $x$  axis in Fig. 2), while the field  $H$  was applied along the  $a$  axis (the  $z$  axis in Fig. 2). Note that the field ( $H = 10$  or 15 T) was applied at high temperatures (at 83 K) and the samples were cooled down to  $\simeq 3$  K using a variable temperature insert (VTI). This procedure ensures that no hysteresis due to the sample is generated.

Temperature steps from  $\simeq 3$  K to 80 K were done

	$L$ (mm)	$w$ (mm)	$t$ (mm)
$\text{TmVO}_4$	0.66	0.24	0.04
$\text{YVO}_4$	0.49	0.25	0.06
$\text{Tm}_{0.7}\text{Y}_{0.3}\text{VO}_4$	0.65	0.45	0.04

TABLE I. Dimensions of the three samples investigated here.  $L$  = length between contacts;  $w$  = width of the sample;  $t$  = thickness of the sample.

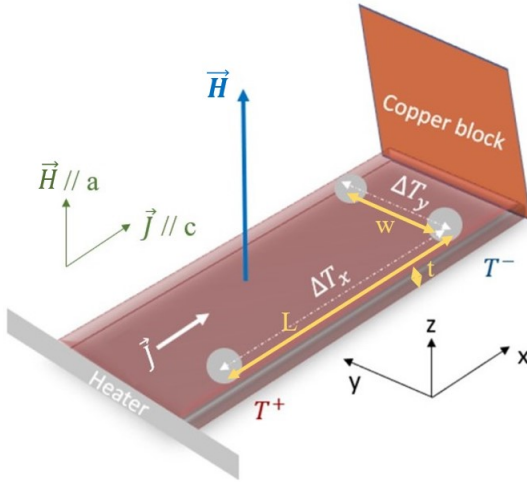


FIG. 2. Experimental setup used to measure  $\kappa_{xx}$  and  $\kappa_{xy}$ . A heat current  $J$  is generated along the  $x$  axis ( $c$  axis of the sample) and a magnetic field  $H$  is applied perpendicular to it, along the  $z$  axis ( $a$  axis of the sample). Differences in temperature are measured along the  $x$  axis (longitudinal temperature difference,  $\Delta T_x = T^+ - T^-$ ) and the  $y$  axis (transverse temperature difference,  $\Delta T_y$ ).

at fixed fields and all the temperature signals were stable before measuring each temperature difference ( $\Delta T_x$  and  $\Delta T_y$  in Fig. 2) using type-E (chromium/constantan) thermocouples. Note that a test has been done previously to show that thermocouples and chip-based thermometers (Cernox) yield the same thermal Hall data (see Appendix C in ref. [33]). Also, note that for all the voltages, the background voltage (when the heat is off) is subtracted from the measured signal (when the heat is on).

The conductivities  $\kappa_{xx}$  and  $\kappa_{xy}$  were measured as described elsewhere [2–4]. Note that the transverse temperature difference  $\Delta T_y$  is obtained by measuring in both field polarities ( $+H$  and  $-H$ ). We have checked that our technique is independent of the particular choice of sequence, i.e., whether we measure  $+H$  first and then  $-H$  or if we measure instead  $-H$  first and then  $+H$ . This means that our experimental setup and our procedure do not generate any (technique dependent) hysteresis. Then, we antisymmetrize the measured signals to get rid of any longitudinal contribution due to a possible slight misalignment of the transverse contacts:

$$\Delta T_y(T, H) = [\Delta T_y(T, H) - \Delta T_y(T, -H)]/2 \quad . \quad (1)$$

The sign of  $\Delta T_y$  is determined by measuring a sample of known  $\kappa_{xy}$  with the same setup and wiring. In a metallic sample with Hall coefficient  $R_H > 0$  (thus an electrical Hall conductivity  $\sigma_{xy} > 0$ ), the thermal Hall conductivity  $\kappa_{xy}$  will be positive (at least in the  $T = 0$  limit) since both thermal and electrical conductivities are related by the Wiedemann–Franz law :  $\kappa_{xy}/T = L_0\sigma_{xy}$  for  $T \rightarrow 0$ .

The thermal conductivity is defined as:

$$\kappa_{xx} = \frac{\dot{Q}}{\Delta T_x \cdot \alpha} \quad , \quad (2)$$

where  $\dot{Q}$  is the heating power and  $\alpha$  is a geometric factor ( $\alpha = \frac{w \cdot t}{L}$ ; see Table I for sample dimensions). The thermal Hall conductivity is defined as:

$$\kappa_{xy} = \kappa_{yy} \left( \frac{\Delta T_y}{\Delta T_x} \right) \left( \frac{L}{w} \right) \quad (3)$$

Note that here we assume that  $\kappa_{yy} = \kappa_{xx}$  (i.e. that  $\kappa_a = \kappa_c$ ), but this is not quite right since the  $c$  axis conductivity is not identical to the  $a$  axis conductivity. This implies that the amplitude of  $\kappa_{xy}$  reported here is not quite accurate, and would need to be multiplied by the anisotropy factor  $\kappa_a/\kappa_c$ . Given the needle shape of our samples, measurements with  $J//a$  have not been done.

### III. RESULTS

#### A. Thermal conductivity, $\kappa_{xx}$

The thermal conductivity  $\kappa_{xx}$  of our three samples is displayed in Fig. 3. All three curves are typical of insulators, with a peak near  $T \simeq 20 - 30$  K.

The thermal conductivity of  $\text{TmVO}_4$  was measured previously [34]. These early measurements were done with  $J//H//c$  (along the easy axis [31]) for  $H < 7$  T and for  $T < 30$  K, whereas our measurements were done with  $J//c$  and  $H//a$ , covering a larger temperature and field range. This previous study reports a slightly higher  $\kappa_{xx}$  peak, perhaps due to larger samples and higher sample quality. The field increased  $\kappa_{xx}$  at low temperatures ( $T < 6$  K).

In our study, we also see an increase in  $\kappa_{xx}$  with  $H$  at low temperatures ( $T < 10$  K; inset of Fig. 4a).

The zero-field curves are compared in Fig. 3(d), where we see that  $\kappa_{xx}$  in  $\text{YVO}_4$  is much larger than in the other two samples. The magnitude of  $\kappa_{xx}$  in the stoichiometric sample of paramagnetic  $\text{TmVO}_4$  is much lower presumably because phonons scatter on the crystal field levels of the  $\text{Tm}^{3+}$  ions. This is also presumed to be the case in the frustrated spin system  $\text{Tb}_2\text{Ti}_2\text{O}_7$ , where the scattering of phonons would involve the crystal field levels of the  $\text{Tb}^{3+}$  ions, as argued previously [8]. This scattering process is much stronger for  $\text{Tb}^{3+}$  than  $\text{Tm}^{3+}$ , resulting in a value of  $\kappa_{xx} \simeq 2 \text{ W/m}\cdot\text{K}$  at  $T = 20$  K in  $\text{Tb}_2\text{Ti}_2\text{O}_7$  [35], compared to  $\kappa_{xx} \simeq 40 \text{ W/m}\cdot\text{K}$  in  $\text{TmVO}_4$  (Fig. 3(a)).

As in the case of  $\text{Tb}_2\text{Ti}_2\text{O}_7$ , where the field dependence of  $\kappa_{xx}$  is exceptionally strong [35], we view the sizable field dependence of  $\kappa_{xx}$  in  $\text{TmVO}_4$  (Fig. 3(a)) and  $\text{Tm}_{0.7}\text{Y}_{0.3}\text{VO}_4$  (Fig. 3(c)), as a confirmation that phonons are scattered by the crystal field levels of the  $\text{Tm}^{3+}$  ions. The weaker field dependence seen in  $\text{YVO}_4$  (Fig. 3(b)) is consistent with that picture. We attribute the fact that  $\kappa_{xx}$  in  $\text{Tm}_{0.7}\text{Y}_{0.3}\text{VO}_4$  is even smaller

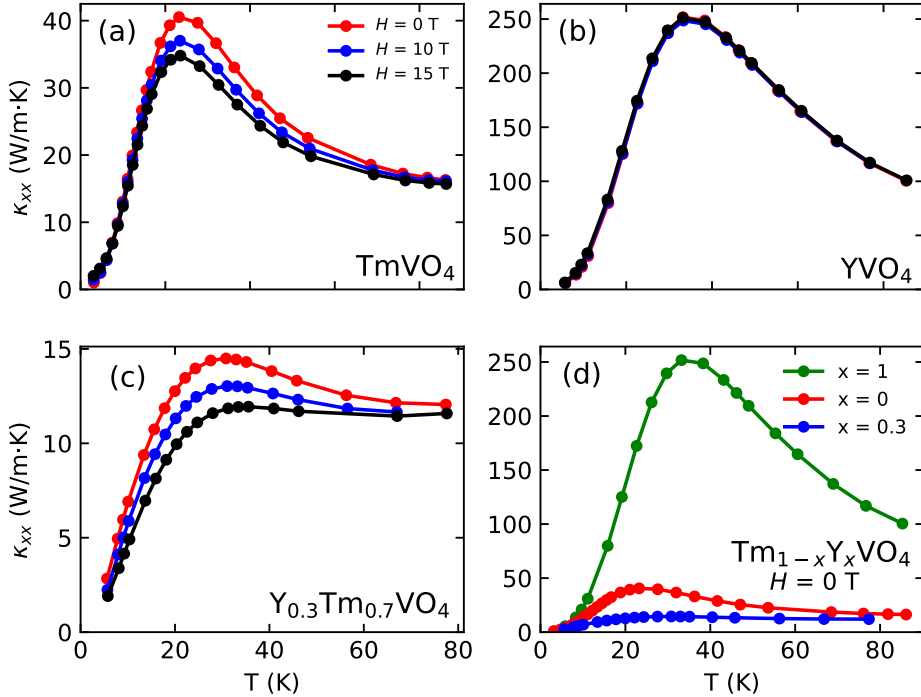


FIG. 3. Thermal conductivity of  $\text{TmVO}_4$  (a),  $\text{YVO}_4$  (b) and  $\text{Y}_{0.3}\text{Tm}_{0.7}\text{VO}_4$  (c) as a function of temperature, measured with a heat current  $J//c$  and a magnetic field  $H//a$  ( $H \perp J$ , for  $H = 0$  (red), 10 T (blue) and 15 T (black)). (d) Comparison of the three conductivities at  $H = 0$ . We see that substituting Y for Tm causes a major reduction in  $\kappa_{xx}$ , which is then further reduced if Y impurities are added.

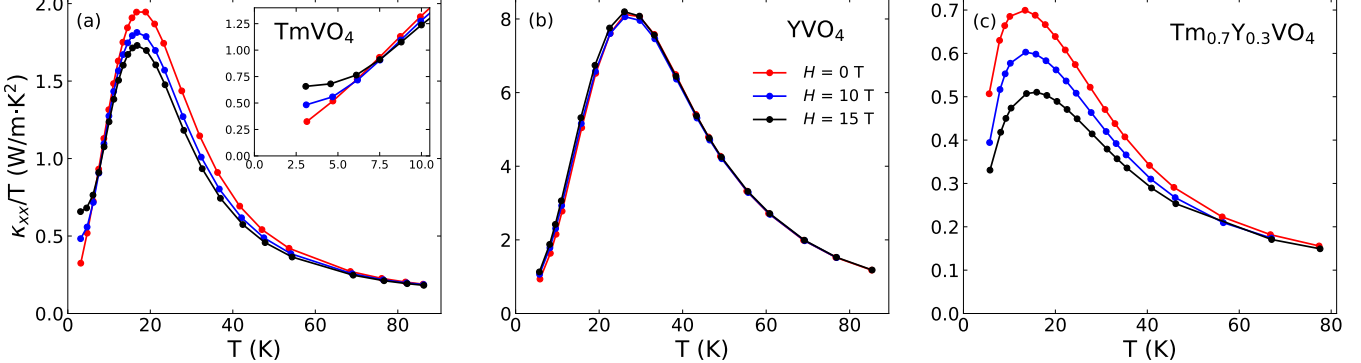


FIG. 4. Thermal conductivity of  $\text{TmVO}_4$  (a),  $\text{YVO}_4$  (b) and  $\text{Tm}_{0.7}\text{Y}_{0.3}\text{VO}_4$  (c), for different applied magnetic fields, as indicated, plotted as  $\kappa_{xx}/T$  vs  $T$  to emphasize the low temperature regime. Note the strong field dependence in the two samples that contain  $\text{Tm}^{3+}$  ions, compared to the much weaker field dependence in  $\text{YVO}_4$ . In panel (a), the inset shows a zoom below 10 K, where we see a different regime of  $H$  dependence, with a strong increase in  $\kappa_{xx}$  with increasing  $H$ .

than in  $\text{TmVO}_4$  to the extra disorder introduced by the Y impurities (Fig. 3(d)).

In Fig. 4, we plot  $\kappa_{xx}/T$  vs  $T$ , to emphasize the data at low temperature. We see that below  $\sim 10$  K or so, the field dependence of  $\kappa_{xx}$  in  $\text{TmVO}_4$  becomes very strong and opposite in sign relative to its behaviour at higher temperature (inset of Fig. 4(a)). We speculate that this change of behaviour is associated with the quadratic splitting of the crystal field levels of the  $\text{Tm}^{3+}$

ions with field (second order Zeeman interaction for  $H // a$ ) [24] which changes the resonant phonon scattering (for phonons of appropriate symmetry).

Interestingly, this change in field dependence as the temperature is raised was actually captured by theoretical calculations that consider the main scattering mechanism of phonons to be resonant scattering on electronic levels of the  $\text{Tm}^{3+}$  ions [36, 37], albeit for temperatures much closer to the transition.

## B. Thermal Hall conductivity, $\kappa_{xy}$

The thermal Hall conductivity  $\kappa_{xy}$  of our three samples is displayed in Fig. 5. Only data at  $H = 15$  T are shown, but data at  $H = 10$  T were also taken; they are similar but smaller in magnitude, roughly in proportion to the field amplitude. The first observation is that all three samples exhibit a non-negligible thermal Hall conductivity. The surprise is that the sign of  $\kappa_{xy}$  is negative in the two stoichiometric materials,  $\text{TmVO}_4$  and  $\text{YVO}_4$ , but it is positive in the disordered sample  $\text{Tm}_{0.7}\text{Y}_{0.3}\text{VO}_4$ .

We see that the temperature at which  $\kappa_{xy}(T)$  peaks (Fig. 5) is the same as the temperature at which the phonon-dominated  $\kappa_{xx}(T)$  peaks (Fig. 3), for example  $\simeq 25$  K in  $\text{TmVO}_4$  and  $\simeq 35$  K in  $\text{YVO}_4$ . As argued before for other materials [4–6, 23], this is an argument in support of phonons being the heat carriers responsible for the thermal Hall signal in these materials.

Looking at Fig. 5, we also notice that the magnitude of  $\kappa_{xy}$  appears to roughly scale with the magnitude of  $\kappa_{xx}$  seen in Fig. 3d. This is confirmed when looking at the thermal Hall angle, plotted as  $|\kappa_{xy}/\kappa_{xx}|$  vs  $T$  in Fig. 6. Indeed, we see that  $|\kappa_{xy}/\kappa_{xx}| \simeq 1 \times 10^{-3}$  at  $T \sim 20$  K in both  $\text{YVO}_4$  and  $\text{Tm}_{0.7}\text{Y}_{0.3}\text{VO}_4$ , even though the magnitude of  $\kappa_{xy}$  is 25 times larger in  $\text{YVO}_4$  (Fig. 5). This is because  $\kappa_{xx}$  is also roughly 25 times larger in  $\text{YVO}_4$  (Fig. 3).

## IV. DISCUSSION

In the pyrochlore study, a non-zero (and positive) thermal Hall effect was measured in  $\text{Tb}_2\text{Ti}_2\text{O}_7$ , but a negligible  $\kappa_{xy}$  was detected in  $\text{Y}_2\text{Ti}_2\text{O}_7$  [17]. It was initially

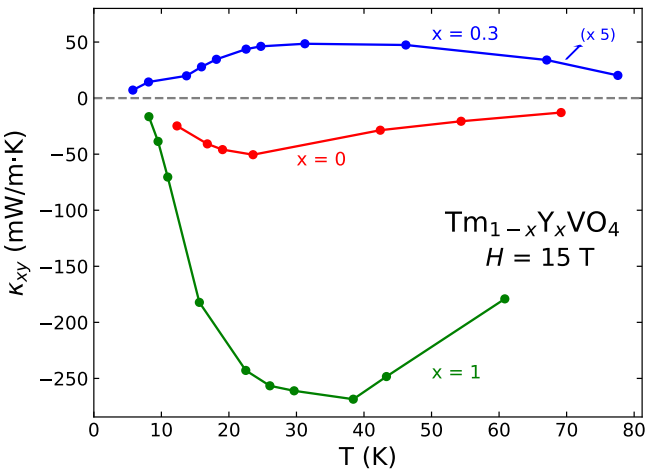


FIG. 5. Thermal Hall conductivity of  $\text{TmVO}_4$  (red),  $\text{YVO}_4$  (green) and  $\text{Tm}_{0.7}\text{Y}_{0.3}\text{VO}_4$  (blue) as a function of temperature, measured with a heat current  $J//c$  and a magnetic field  $H//a$  ( $H \perp J$ ), at  $H = 15$  T. Note that  $\kappa_{xy}$  for  $\text{Tm}_{0.7}\text{Y}_{0.3}\text{VO}_4$  has been multiplied by a factor of 5.

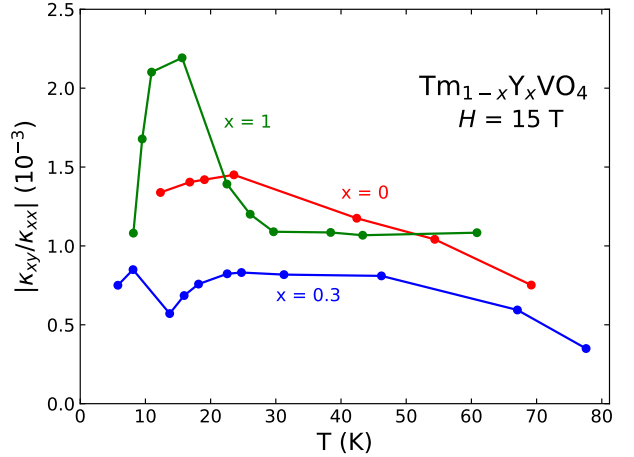


FIG. 6. Thermal Hall angle of  $\text{TmVO}_4$  (red),  $\text{YVO}_4$  (green) and  $\text{Tm}_{0.7}\text{Y}_{0.3}\text{VO}_4$  (blue), plotted as  $|\kappa_{xy}/\kappa_{xx}|$  vs  $T$ , for  $H = 15$  T. At  $T = 20$  K, the obtained value is around  $1 \times 10^{-3}$  for all three materials, a magnitude typical of the phonon Hall effect in several insulators [6, 23].

speculated that the thermal Hall signal in  $\text{Tb}_2\text{Ti}_2\text{O}_7$  was due to some exotic spin excitations [17]. However, a subsequent study found that the  $\kappa_{xy}$  signal remains as strong when 70% of the magnetic  $\text{Tb}^{3+}$  ions are replaced by nonmagnetic  $\text{Y}^{3+}$  ions, thereby dramatically altering the frustrated spin-liquid state of pure  $\text{Tb}_2\text{Ti}_2\text{O}_7$  [18]. This led to the conclusion that phonons are in fact the heat carriers responsible for the thermal Hall effect in these pyrochlores. Moreover, the fact that  $\kappa_{xy}$  becomes negligible in  $\text{Y}_2\text{Ti}_2\text{O}_7$ , when all Tb is replaced by Y, indicates that magnetism plays a key role in the generation of the phonon thermal Hall effect in these pyrochlores.

Turning to our own study, we also observe a non-zero  $\kappa_{xy}$  in  $\text{TmVO}_4$ , another oxide with magnetic ions ( $\text{Tm}^{3+}$ ), and we also attribute this Hall effect to phonons, as argued above. In our comparison with  $\text{Tb}_2\text{Ti}_2\text{O}_7$ , we see two differences. The first is the fact that our nonmagnetic parent compound,  $\text{YVO}_4$ , also displays a non-zero  $\kappa_{xy}$ , unlike the negligible signal of  $\text{Y}_2\text{Ti}_2\text{O}_7$ . So in these vanadates, the phonon Hall effect does not depend crucially on the magnetic moment associated with  $\text{Tm}^{3+}$  ions. Note that a non-zero thermal Hall effect from phonons has been observed in other nonmagnetic insulators, such as strontium titanate [5] and black phosphorous [23].

The second difference is the sign of  $\kappa_{xy}$ : positive in  $\text{Tb}_2\text{Ti}_2\text{O}_7$ , negative in  $\text{TmVO}_4$ . The sign of the phonon Hall conductivity is an entirely open question, on which existing theories shed little light. Phenomenologically, both signs are observed, see Fig. 1. For example, the phononic  $\kappa_{xy}$  is negative in  $\text{SrTiO}_3$  [5],  $\text{Cu}_3\text{TeO}_6$  [6] and black phosphorous [23], as well as in all cuprates, whether undoped [3, 4], hole-doped [2] or electron-doped [20]. A positive phononic  $\kappa_{xy}$  is observed in  $\text{Fe}_2\text{Mo}_3\text{O}_8$  [1],  $(\text{Tb}_{0.3}\text{Y}_{0.7})_2\text{Ti}_2\text{O}_7$  [18] and  $\text{RuCl}_3$  [19, 38]. A remarkable

feature of our findings is that  $\kappa_{xy}$  changes sign to positive upon introducing 30% Y into  $\text{TmVO}_4$  (Fig. 5). This suggests that impurities, in much larger concentration in  $\text{Tm}_{0.7}\text{Y}_{0.3}\text{VO}_4$  relative to either  $\text{TmVO}_4$  or  $\text{YVO}_4$ , is an important ingredient for the generation of a phonon thermal Hall effect.

It is instructive to look at the magnitude of  $\kappa_{xy}$ . As argued by others [1, 6, 23], the relevant quantity for this is the ratio  $\kappa_{xy}/\kappa_{xx}$ , namely the Hall angle. In Fig. 6, we see that in our three samples  $|\kappa_{xy}/\kappa_{xx}| \simeq 1 \times 10^{-3}$  at  $T = 20$  K and  $H = 15$  T. This is quite typical. Indeed, the cuprate Mott insulators  $\text{La}_2\text{CuO}_4$ ,  $\text{Nd}_2\text{CuO}_4$  and  $\text{Sr}_2\text{CuO}_2\text{Cl}_2$  and the antiferromagnetic insulator  $\text{Cu}_3\text{TeO}_6$  all have a Hall angle of about  $3 \times 10^{-3}$  at the same temperature and field [6]. The Kitaev spin liquid candidate  $\text{RuCl}_3$  has a Hall angle of about  $1 \times 10^{-3}$ . Note that the magnitude of  $\kappa_{xy}$  varies by three orders of magnitude across those various materials.

It is worth noting that significantly larger thermal Hall angles have been observed in two cases so far: the Ce-doped cuprate  $\text{Nd}_2\text{CuO}_4$  [20] and the Rh-doped iridate  $\text{Sr}_2\text{IrO}_4$  [21]. In as-grown samples of  $\text{Nd}_2\text{CuO}_4$  with 11% Ce and  $\text{Sr}_2\text{IrO}_4$  with 5% Rh,  $|\kappa_{xy}/\kappa_{xx}| \simeq 30 \times 10^{-3}$  at  $T = 20$  K and  $H = 15$  T. Both materials are insulators with antiferromagnetic order at these dopings, and it was argued in the latter study that impurities embedded in an antiferromagnetic environment strongly promote the phonon thermal Hall effect [21], as suggested theoretically for a mechanism of resonant side-jump scattering of phonons [16].

## V. SUMMARY

We have measured a non-zero thermal Hall conductivity  $\kappa_{xy}$  in the vanadates  $\text{TmVO}_4$ ,  $\text{YVO}_4$  and  $\text{Tm}_{0.7}\text{Y}_{0.3}\text{VO}_4$ . All evidence points to phonons as the heat carriers responsible for generating this Hall effect. The magnitude of the Hall response is similar in all three, with a Hall angle of  $|\kappa_{xy}/\kappa_{xx}| \simeq 1 \times 10^{-3}$  at  $T = 20$  K and  $H = 15$  T, comparable to the phonon Hall effect in several insulating materials. This shows that  $\text{Tm}^{3+}$  ions do not play an essential role in generating the Hall effect in these rare-earth vanadates. While the sign of  $\kappa_{xy}$  in the two stoichiometric compounds  $\text{TmVO}_4$  and  $\text{YVO}_4$  is negative, we find a positive sign in the more disordered  $\text{Tm}_{0.7}\text{Y}_{0.3}\text{VO}_4$ . This points to a special role played by impurities in this family of materials.

## ACKNOWLEDGMENTS

We thank S. Fortier for his assistance with the experiments. L. T. acknowledges support from the Canadian Institute for Advanced Research (CIFAR) as a CIFAR Fellow and funding from the Institut Quantique, the Natural Sciences and Engineering Research Council of Canada (NSERC; PIN:123817), the Fonds de Recherche

du Québec - Nature et Technologies (FRQNT), the Canada Foundation for Innovation (CFI), and a Canada Research Chair. This research was undertaken thanks in part to funding from the Canada First Research Excellence Fund.

Crystal growth and characterization performed at Stanford University was supported by the Air Force Office of Scientific Research under award number FA9550-20-1-0252. MPZ was also partially supported by a National Science Foundation Graduate Research Fellowship under grant number DGE-1656518.

## APPENDIX

The thermal Hall effect can be measured in three ways and we have tested these methods on the hole-doped cuprate  $\text{La}_{2-x}\text{Sr}_x\text{CuO}_4$   $p = 0.06$  (LSCO):

1) Steady-state method as function of temperature, also known as “ $T$ -steps” (see Fig. 7 and Fig. 8). The magnetic field  $H$  is kept fixed while the temperature  $T$  of the sample is changed in discrete steps (2-3 K steps). At each temperature, the background voltage of the thermocouple that measures  $\Delta T_y$  is recorded before the heat  $\dot{Q}$  is applied to the sample. When the sample is in an equilibrium configuration,  $\Delta T_y(H)$  is measured.

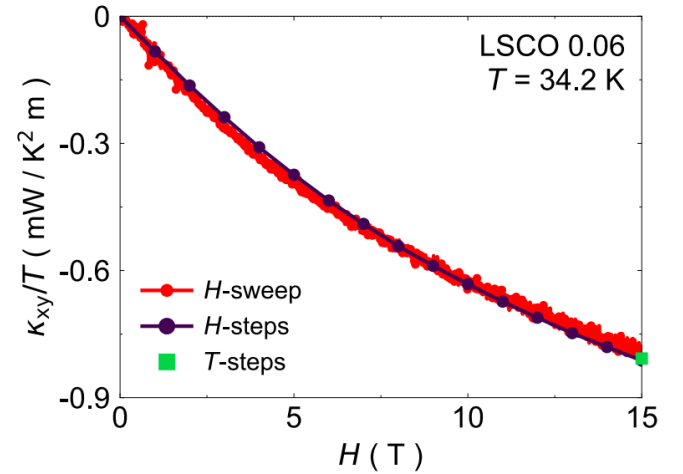


FIG. 7.  $\kappa_{xy}/T$  as a function of magnetic field  $H$  at fixed  $T = 34.2$  K in the hole-doped cuprate  $\text{La}_{2-x}\text{Sr}_x\text{CuO}_4$   $p = 0.06$  (LSCO). The red circles are obtained sweeping the magnetic field continuously at a rate of 0.7 T/min. The purple circles are obtained using a steady-state method as a function of field with steps of 1 T. The green square is obtained using a steady-state method as a function of temperature at  $H = 15$  T.

The background voltage of the thermocouple is carefully subtracted from the measured heat-on signal from the thermocouple. Once the entire temperature range is covered, say from 10 K to 100 K, the field direction is reversed to  $-H$ . The same procedure is followed for

this field polarity. Then, the  $\Delta T_y$  signal is antisymmetrized;  $\Delta T_y(T, H) = [\Delta T_y(T, H) - \Delta T_y(T, -H)]/2$ , such that any symmetric contribution, coming from the longitudinal thermal gradient due to misalignment of the transverse contacts, is removed.

2) Steady-state method as a function of field, also known as “ $H$ -steps” (see Fig. 7 and Fig. 8). The temperature  $T$  is kept fixed, and the magnetic field  $H$  is changed in discrete steps (1-2 T steps). At a fixed temperature, a heat current  $\bar{J}$  is sent to the sample, and once it reaches equilibrium, the magnetic field is changed from  $H$  to  $-H$  in steps. For each field step  $h$ , we define  $\Delta T_y(T, h) = [\Delta T_y(T, h) - \Delta T_y(T, -h)]/2$ . Once the entire magnetic field range is covered, the temperature of the sample is changed and the same procedure is repeated.

3) Field sweep method, also known as “ $H$ -sweeps” (see Fig. 7). This method is similar to 2), but now the magnetic field is continuously changed from  $H$  to  $-H$ .

We have found satisfactory agreement between methods 1), 2) and 3), see Fig. 7.

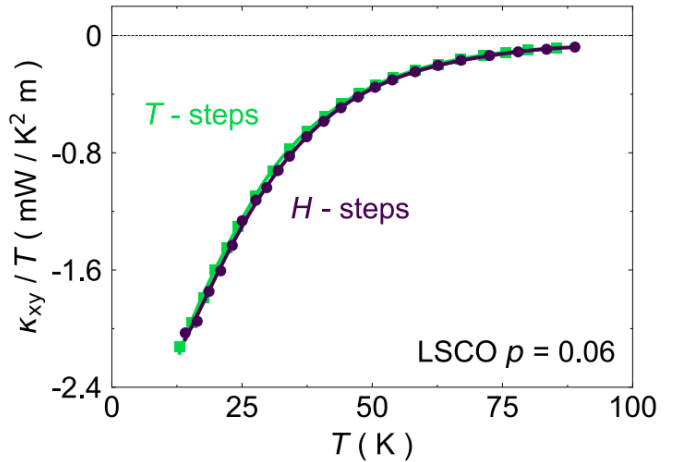


FIG. 8.  $\kappa_{xy}/T$  as a function of temperature at  $H = 15$  T in the hole-doped cuprate  $\text{La}_{2-x}\text{Sr}_x\text{CuO}_4$   $p = 0.06$  (LSCO). The green squares are obtained using a steady-state method as a function of temperature. The purple circles are obtained using a steady-state method as a function of magnetic field.

---

[1] T. Ideue, T. Kurumaji, S. Ishiwata, and Y. Tokura, Giant thermal Hall effect in multiferroics, *Nature Materials* **16**, 797 (2017).

[2] G. Grissonnanche, A. Legros, S. Badoux, E. Lefrançois, V. Zatko, M. Lizaire, F. Laliberté, A. Gourgout, J.-S. Zhou, S. Pyon, T. Takayama, H. Takagi, S. Ono, N. Doiron-Leyraud, and L. Taillefer, Giant thermal Hall conductivity in the pseudogap phase of cuprate superconductors, *Nature* **571**, 376 (2019).

[3] G. Grissonnanche, S. Thériault, A. Gourgout, M.-E. Boulanger, E. Lefrançois, A. Ataei, F. Laliberté, M. Dion, J.-S. Zhou, S. Pyon, T. Takayama, H. Takagi, S. Ono, N. Doiron-Leyraud, and L. Taillefer, Chiral phonons in the pseudogap phase of cuprates, *Nature Physics* **16**, 1108 (2020).

[4] M.-E. Boulanger, G. Grissonnanche, S. Badoux, A. Alalaire, E. Lefrançois, A. Legros, A. Gourgout, M. Dion, C. H. Wang, X. H. Chen, R. Liang, W. N. Hardy, D. A. Bonn, and L. Taillefer, Thermal Hall conductivity in the cuprate Mott insulators  $\text{Nd}_2\text{CuO}_4$  and  $\text{Sr}_2\text{CuO}_2\text{Cl}_2$ , *Nature Communications* **11**, 5325 (2020).

[5] X. Li, B. Fauqué, Z. Zhu, and K. Behnia, Phonon thermal Hall effect in strontium titanate, *Physical Review Letters* **124**, 105901 (2020).

[6] L. Chen, M.-E. Boulanger, Z.-C. Wang, F. Tafti, and L. Taillefer, Large phonon thermal Hall conductivity in the antiferromagnetic insulator  $\text{Cu}_3\text{TeO}_6$ , *Proceedings of the National Academy of Sciences* **119**, e2208016119 (2022).

[7] C. Strohm, G. L. J. A. Rikken, and P. Wyder, Phenomenological evidence for the phonon Hall effect, *Physical Review Letters* **95**, 155901 (2005).

[8] M. Mori, A. Spencer-Smith, O. P. Sushkov, and S. Maekawa, Origin of the phonon Hall effect in rare-earth garnets, *Physical Review Letters* **113**, 265901 (2014).

[9] T. Qin, J. Zhou, and J. Shi, Berry curvature and the phonon Hall effect, *Physical Review B* **86**, 104305 (2012).

[10] M. Ye, L. Savary, and L. Balents, Phonon Hall viscosity in magnetic insulators, *arXiv [Preprint]* (2021), arXiv:2103.04223.

[11] Y. Zhang, Y. Teng, R. Samajdar, S. Sachdev, and M. S. Scheurer, Phonon Hall viscosity from phonon-spinon interactions, *Physical Review B* **104**, 035103 (2021).

[12] R. Samajdar, S. Chatterjee, S. Sachdev, and M. S. Scheurer, Thermal Hall effect in square-lattice spin liquids: A Schwinger boson mean-field study, *Physical Review B* **99**, 165126 (2019).

[13] L. Mangeolle, L. Balents, and L. Savary, Phonon thermal Hall conductivity from scattering with collective fluctuations, *Physical Review X* **12**, 041031 (2022).

[14] H. Guo and S. Sachdev, Extrinsic phonon thermal Hall transport from Hall viscosity, *Physical Review B* **103**, 205115 (2021).

[15] X.-Q. Sun, J.-Y. Chen, and S. A. Kivelson, Large extrinsic phonon thermal Hall effect from resonant scattering, *Physical Review B* **106**, 144111 (2022).

[16] H. Guo, D. G. Joshi, and S. Sachdev, Resonant thermal Hall effect of phonons coupled to dynamical defects, *Proceedings of the National Academy of Sciences* **119**, e2215141119 (2022).

[17] M. Hirschberger, J. W. Krizan, R. J. Cava, and N. P. Ong, Large thermal Hall conductivity of neutral spin excitations in a frustrated quantum magnet, *Science* **348**, 106 (2015).

[18] Y. Hirokane, Y. Nii, Y. Tomioka, and Y. Onose, Phononic thermal Hall effect in diluted terbium oxides, *Physical Review B* **99**, 134419 (2019).

[19] E. Lefrançois, G. Grissonnanche, J. Baglo, P. Lampen-

Kelley, J.-Q. Yan, C. Balz, D. Mandrus, S. E. Nagler, S. Kim, Y.-J. Kim, N. Doiron-Leyraud, and L. Taillefer, Evidence of a phonon Hall effect in the Kitaev spin liquid candidate  $\alpha$ -RuCl<sub>3</sub>, *Physical Review X* **12**, 021025 (2022).

[20] M.-E. Boulanger, G. Grissonnanche, E. Lefrançois, A. Gourgout, K.-J. Xu, Z.-X. Shen, R. L. Greene, and L. Taillefer, Thermal Hall conductivity of electron-doped cuprates, *Physical Review B* **105**, 115101 (2022).

[21] A. Ataei, G. Grissonnanche, M.-E. Boulanger, L. Chen, E. Lefrançois, V. Brouet, and L. Taillefer, Phonon chirality from impurity scattering in the antiferromagnetic phase of Sr<sub>2</sub>IrO<sub>4</sub>, *Nature Physics* (2024).

[22] Q. Meng, X. Li, L. Zhao, C. Dong, Z. Zhu, and K. Behnia, Thermal Hall effect driven by phonon-magnon hybridization in a honeycomb antiferromagnet, arXiv [Preprint] (2024), arXiv:2403.13306.

[23] X. Li, Y. Machida, A. Subedi, Z. Zhu, L. Li, and K. Behnia, The phonon thermal Hall angle in black phosphorus, *Nature Communications* **14**, 1027 (2023).

[24] I. Vinograd, K. R. Shirer, P. Massat, Z. Wang, T. Kissikov, D. Garcia, M. D. Bachmann, M. Horvatić, I. R. Fisher, and N. J. Curro, Second order Zeeman interaction and ferroquadrupolar order in TmVO<sub>4</sub>, *NPJ Quantum Materials* **7**, 1 (2022).

[25] Z. Wang, I. Vinograd, Z. Mei, P. Menegasso, D. Garcia, P. Massat, I. R. Fisher, and N. J. Curro, Anisotropic nematic fluctuations above the ferroquadrupolar transition in TmVO<sub>4</sub>, *Physical Review B* **104**, 205137 (2021).

[26] P. Massat, J. Wen, J. M. Jiang, A. T. Hristov, Y. Liu, R. W. Smaha, R. S. Feigelson, Y. S. Lee, R. M. Fernandes, and I. R. Fisher, Field-tuned ferroquadrupolar quantum phase transition in the insulator TmVO<sub>4</sub>, *Proceedings of the National Academy of Sciences* **119**, e2119942119 (2022).

[27] Y.-H. Nian, I. Vinograd, T. Green, C. Chaffey, P. Massat, R. R. P. Singh, M. P. Zic, I. R. Fisher, and N. J. Curro, Spin-echo and quantum versus classical critical fluctuations in TmVO<sub>4</sub>, arXiv [Preprint] (2023), arXiv:2306.13244.

[28] M. P. Zic, M. S. Ikeda, P. Massat, P. M. Hollister, L. Ye, E. W. Rosenberg, J. A. W. Straquadine, B. J. Ramshaw, and I. R. Fisher, Giant elastocaloric effect at low temperatures in TmVO<sub>4</sub> and implications for cryogenic cooling, arXiv [Preprint] (2023), arXiv:2308.15577.

[29] R. Feigelson, Flux growth of type RVO<sub>4</sub> rare-earth vanadate crystals, *Journal of the American Ceramic Society* **51**, 538 (1968).

[30] S. H. Smith and B. M. Wanklyn, Flux growth of rare earth vanadates and phosphates, *Journal of Crystal Growth* **21**, 23 (1974).

[31] H. Suzuki, T. Inoue, and T. Ohtsuka, Enhanced nuclear cooling and spin-lattice relaxation time in TmVO<sub>4</sub> and TmPO<sub>4</sub>, *Physica B+C* **107**, 563 (1981).

[32] A. H. Cooke, S. J. Swindenby, and M. R. Wells, The properties of thulium vanadate — An example of molecular field behaviour, *Solid State Communications* **10**, 265 (1972).

[33] G. Grissonnanche, F. Laliberté, S. Dufour-Beauséjour, M. Matusiak, S. Badoux, F. F. Tafti, B. Michon, A. Ropel, O. Cyr-Choinière, J. C. Baglo, B. J. Ramshaw, R. Liang, D. A. Bonn, W. N. Hardy, S. Krämer, D. LeBoeuf, D. Graf, N. Doiron-Leyraud, and L. Taillefer, Wiedemann-Franz law in the underdoped cuprate superconductor YBa<sub>2</sub>Cu<sub>3</sub>O<sub>y</sub>, *Physical Review B* **93**, 064513 (2016).

[34] B. Daudin and B. Salce, Thermal conductivity of rare earth vanadates and arsenates undergoing a cooperative Jahn-Teller effect, *Journal of Physics C: Solid State Physics* **15**, 463–475 (1982).

[35] Q. J. Li, Z. Y. Zhao, C. Fan, F. B. Zhang, H. D. Zhou, X. Zhao, and X. F. Sun, Phonon-glass-like behavior of magnetic origin in single-crystal Tb<sub>2</sub>Ti<sub>2</sub>O<sub>7</sub>, *Physical Review B* **87**, 214408 (2013).

[36] W. Mutscheller and M. Wagner, Thermal conductivity of cooperative Jahn-Teller E-systems, *Physica Status Solidi (b)* **134**, 39 (1986).

[37] W. Mutscheller and M. Wagner, The influence of magnetic fields on the thermal conductivity of the cooperative vibronic system TmVO<sub>4</sub>, *Physica Status Solidi (b)* **144**, 507 (1987).

[38] R. Henrich, M. Roslova, A. Isaeva, T. Doert, W. Brenig, B. Büchner, and C. Hess, Large thermal Hall effect in  $\alpha$ -RuCl<sub>3</sub>: Evidence for heat transport by Kitaev-Heisenberg paramagnons, *Physical Review B* **99**, 085136 (2019).